

# Deliverable 3.2.1

Author: Joseba Moreno, Max Schmid

Release Status: FINAL

Date: 12 August 2020

Filename and version: NEWEST\_D3.2.1\_USTUTT



ACT2 NEWEST-CCUS project No 299683

This project NEWEST-CCUS is funded through the ACT programme (Accelerating CCS Technologies). Financial contributions made from The Research Council of Norway, (RCN), Norway; Bundesministerium für Wirtschaft und Energie (BMWi), Germany; Netherlands Enterprise Agency (RVO), Netherlands; and Department for Business, Energy & Industrial Strategy (BEIS) together with the Natural Environment Research Council (NERC) and the Engineering and Physical Sciences Research Council (EPSRC), United Kingdom are gratefully acknowledged.



This work was jointly supported by the Federal Ministry for Economic Affairs and Energy (BMWi).



# Document History

## Location

This document is stored in the following location:

Filename	NEWEST_D3.2.1_USTUTT
Location	SCCS shared drive

## Revision History

This document has been through the following revisions:

Version No.	Revision Date	Filename/Location stored:	Brief Summary of Changes
Version 1	12/08/2020	NEWEST_D3.2.1_USTUTT	

## Authorisation

This document requires the following approvals:

AUTHORISATION	Name	Signature	Date
WP Leader or co-leader	Mario Ditaranto, Max Schmid		
Project Coordinator	Mathieu Luquiaud		29/11/2022

## Distribution

This document has been distributed to:

Name	Title	Version Issued	Date of Issue
			00/00/0000

© NEWEST-CCUS project, 2020

No third-party textual or artistic material is included in the publication without the copyright holder's prior consent to further dissemination by other third parties.

Reproduction is authorised provided the source is acknowledged.

### **Disclaimer**

The information and views set out in this deliverable are those of the author(s) and do not necessarily reflect the official opinion of the Funders (RCN, BMWi, RVO, BEIS with NERC and EPSRC). Neither the Funders and bodies nor any person acting on their behalf may be held responsible for the use which may be made of the information contained therein.

# Executive Summary

Within the NEWEST-CCUS project (Project-Nr.: 299683) different carbon capture, usage and storage (CCUS) technologies are to be investigated in the context of Waste-to-Energy (WtE) plants, aiming at achieving net negative CO<sub>2</sub> emissions.

A promising possibility in this regard comprise oxy-firing technologies applied to fluidised bed systems, which introduce the potential for higher efficiency with solid recovered fuel (SRF) combustion. During oxy-fuel combustion, the fuel is fired using pure oxygen instead of air as the primary oxidant. Since the nitrogen component of air is not heated, fuel consumption is reduced and higher flame temperatures are possible. The justification for using oxy-fuel is thus to produce a CO<sub>2</sub> rich flue gas ready for sequestration.

In this document results from lab-scale BFB combustion experiments under air and oxy-fuel firing conditions are presented. Cold dosing experiments of four SRF candidates have been investigated in a first phase of the tests. A pelletised SRF from Spain (i.e. ECO-P) has been then used for the air and oxy-fuel combustion experiments. In the air combustion experiments, the influence of the reactor temperature over the ash behavior and flue gas species has been investigated. For the oxy-fuel tests, the same process evaluation has been performed, though at a reference temperature (i.e. 850 °C) and at different inlet oxygen concentrations (i.e. 21 vol%<sub>db</sub>, 30 vol%<sub>db</sub> and 40 vol%<sub>db</sub>).

The results show, that the observed pilot data during both combustion modes matches reasonably well to the results obtained from stoichiometric combustion equations and process simulations. Combustion of pelletised SRF shows to be feasible with the current experimental set up at the 20 kW BFB reactor, without technical limitations posed by bed agglomeration issues, even after a few hours of continuous operation.

# Table of Contents

<b>Executive Summary</b> .....	<b>4</b>
<b>List of abbreviations</b> .....	<b>6</b>
<b>List of symbols</b> .....	<b>7</b>
<b>1 The waste to energy (WtE) conversion process</b> .....	<b>8</b>
<b>2 The oxy-fuel technology</b> .....	<b>8</b>
2.1 Oxy-fuel applied to WtE plants .....	9
<b>3 Oxy-fuel combustion pre-tests at USTUTT</b> .....	<b>10</b>
3.1 Experimental facility .....	10
3.2 Materials .....	11
3.2.1 Bed material .....	11
3.2.2 Fuels .....	12
<b>4 Cold dosing experiments</b> .....	<b>13</b>
4.1 Methodology .....	13
4.2 Results .....	14
4.2.1 SBS-2 .....	14
4.2.2 CHEM .....	15
4.2.3 SBS-1 .....	15
<b>5 Combustion experiments</b> .....	<b>15</b>
5.1 Air combustion tests .....	15
5.1.1 Experimental parameters .....	16
5.1.2 Results .....	16
5.2 Oxy-fuel combustion tests .....	20
5.2.1 Experimental parameters .....	20
5.2.2 Results .....	21
<b>6 Conclusions and Outlook</b> .....	<b>26</b>
<b>Acknowledgements</b> .....	<b>26</b>
<b>References</b> .....	<b>27</b>
<b>Annex</b> .....	<b>28</b>

## List of abbreviations

Acronym	Description
a.r.	As received
ASU	Air separation unit
BFB	Bubbling fluidised bed
BFBC	Bubbling fluidised bed combustor
CCS	Carbon capture and storage
CCUS	Carbon capture, utilisation and storage
CFB	Circulating fluidised bed
CPU	Compression and purification unit
db	Dry basis
FBC	Fluidised bed combustion
FTIR	Fourier-transform infrared spectroscopy
GHG	Greenhouse gas(es)
LCV	Low calorific value
MSW	Municipal solid waste
PC	Pulverised coal
PSD	Particle size distribution
RFG	Recirculated flue gas
SRF	Solid recovered fuel
waf	Water and ash free
wf	Water free
WIP	Waste incineration plant
WtE	Waste to energy

## List of symbols

Symbol	Description
$M$	Mass (kg)
$\dot{M}$	Mass flow rate (kg/h)
$M_i$	Molecular mass of component "i" (kg/mol)
$n$	Air excess ratio
$\Delta n$	Excess air
$P$	Pressure (mbar)
$q_3(x)$	Frequency distribution (%)
$Q_3(x)$	Cumulative distribution (%)
$u$	Gas superficial velocity (m/s)
$\dot{V}$	Volume flow rate (kg/h)
$V_{mn}$	Molar volume (STP)
$x_i$	Mass fraction of component "i" (kg/kg)
$y_i$	Gas volume fraction of component "i" (vol% or ppm)
$\mu_i$	Specific mass of component "i" (kg/kg)
$\rho_i$	Density of component "i" (kg/m <sup>3</sup> )
$\gamma_i$	Fuel mass fraction of component "i" (kg/kg)
$\vartheta$	Temperature (°C)

## 1 The waste to energy (WtE) conversion process

Rising industrialisation, population growth and the environmental concerns arising from inadequate waste disposal are leading to an increasing global scale motivation for recovering energy from municipal solid waste (MSW). The use of MSW can contribute to the increase of renewable energy share in the final energy production, decreasing the volume of solid waste dumped in landfills and reducing the global GHG emissions through improved solid waste management.

The European Commission has developed an action plan with objectives and targets to improve waste management, as well as to reduce GHG emissions and adverse health and environmental impacts [6]. This communication introduces a legally binding prioritisation of waste management activities, where waste prevention is the most desirable option, followed by material recovery and recycling, energy recovery from waste and finally disposal (landfilling) without recovery of either materials and/or energy. Despite the large drop regarded in the landfilling rates compared to MSW generation, a large share (>30 %) of the EU's municipal waste is still being landfilled [12]. This suggests that the recovery of energy from MSW has a huge potential to become an important player in the European renewable energy sector. Nonetheless, rough estimates show that CO<sub>2</sub> emissions from waste incineration still account for around 2% of the overall GHG emissions from the waste sector [4]. Considerable measures that can reduce CO<sub>2</sub> emissions in this context comprise i) the rapid and strong deployment of renewable or nuclear energy; ii) an increase of the waste fuel conversion efficiency and iii) the application of Carbon Capture, Utilisation and Storage (CCUS) technologies. Since option i) is currently not available in an extent that allows to supply the global energy demand and option ii) is limited in its overall CO<sub>2</sub> emission reduction potential, the application of CCUS technologies (or just CCS) seems to be mandatory to reach the CO<sub>2</sub> reduction goals.

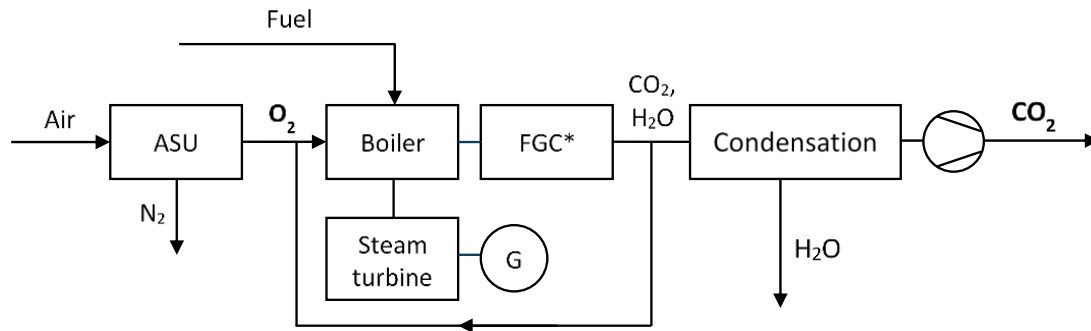
A promising CCS candidate in this regard is the oxy-fuel combustion technology. Among all the available CCS options (i.e. pre-combustion, post-combustion and oxy-fuel), combustion with pure oxygen is commonly regarded as the best solution for achieving near-zero CO<sub>2</sub> emission power generation in the foreseeable future. The application of this technology indeed reduces the volume of flue gas (by about 75%), increases the boiler efficiency, reduces the formation of nitrogen oxides (NO<sub>x</sub>) and allows for high fuel flexibility, among others [9].

## 2 The oxy-fuel technology

Oxy-fuel combustion combined with CO<sub>2</sub> storage is being globally recognised as a promising technology which can enable the continuous use of stationary combustion plants during the period of transition to renewable energy sources. The process refers to a fuel being burned in an enriched oxygen atmosphere to obtain high CO<sub>2</sub> concentrations in the exhaust flue gas, which are suitable for capture after prior purification and compression.

Unlike conventional air combustion plants which use air (O<sub>2</sub>/N<sub>2</sub>) as the oxidant, an oxy-fired plant employs an air separation unit (ASU) to produce an almost pure oxygen stream. The oxygen is then combined with recirculated flue gas (RFG) to produce an oxygen enriched gas as the oxidant (O<sub>2</sub>/CO<sub>2</sub>, O<sub>2</sub> concentration > 21 vol%<sub>db</sub>). RFG is necessary to moderate the combustion flame temperature. After combustion, the flue gas is purified in a dust elimination unit, followed by further purification, i.e. removal of water and other gas impurities, and compression (CPU). This results in nearly-zero carbon emissions, as the CO<sub>2</sub> generated by oxy-fuel combustion is separated and collected with a high purity degree (CO<sub>2</sub> concentration up to 95 vol%<sub>db</sub>). A simplified schematic of an oxy-fuel combustion system with flue-gas recirculation is shown in \* FGC: Flue Gas Cleaning

Figure 1.



\* FGC: Flue Gas Cleaning

Figure 1. Simplified schematic of the oxy-fuel combustion process.

There are two approaches which can be applied to the oxy-fuel combustion process: i) pulverised coal combustion (PC) and ii) fluidised bed boiler combustion (FBC). FBC is characterised for offering a better performance than PC boilers in terms of fuel adaptability (i.e. flexibility), combustion intensity,  $\text{NO}_x$  emissions and process control characteristics [11]. Among the different FBC options, circulating fluidised bed (CFB) combustion has attracted increasing attention globally due to relevant advantages, such as: i) the reduction in the combustion energy of recirculated gas due to the higher oxygen concentrations applied in the process; and ii) the possibility for lower excess oxygen levels compared to PC boilers, decreasing hereby the energy consumption in the ASU unit.

## 2.1 Oxy-fuel applied to WtE plants

Even if the feasibility of the oxy-fuel (pulverised) coal and biomass combustion has already been investigated at laboratory and pilot-scale in several projects worldwide [7,8,10,13], its integration into the waste combustion system has not been assessed in detail yet. Indeed, the application of the oxy-fuel technology to the waste-to-energy sector requires clarification in several process aspects [5], such as: i) MSW combustion properties under oxy-fuel combustion conditions; ii) construction of reliable combustion modelling tools; or iii) the effect of oxygen purity and iv) air leakage issues on the combustion process.

Currently, there are several projects aiming at addressing the above mentioned aspects experimentally (e.g. CapeWaste, MONIKA). Additionally, several industrial companies are already working on providing technical solutions (i.e. waste incinerators) with similar characteristics as the oxy-fuel technology (e.g. Martin GmbH, Steinmüller Engineering GmbH). Thanks to this growing interest in the oxy-fuel combustion, the process has seen considerable improvement in the last decades and is still expected to gain another 10-15% efficiency points in the coming years [5]. Most research is being carried out towards the ASU unit, as this constitutes most of the energy penalty incurred by the technology. Also the CPU has been proven to be very efficient by combining compression and pollutants cleaning in an integrated unit.

Last but not least, and from a technological point of view, the application of the oxy-fuel combustion process to WtE plants offers several advantages in front of air combustion [14]. It allows for a well-designed oxygen distribution in the boiler, which enables accommodation of in real time process fluctuations and/or inhomogeneities of low-quality fuels.

### 3 Oxy-fuel combustion pre-tests at USTUTT

#### 3.1 Experimental facility

The 20 kW fuel input fluidised bed facility used during the oxy-fuel combustion pre-tests is shown in Figure 2. 20 kW bubbling fluidised bed . The bubbling fluidised bed (BFB) reactor has a total internal height of 3.5 m with an internal diameter of 150 mm in the combustion zone and 200 mm in the freeboard above.

The facility is equipped with various thermocouples and pressure transducers to ensure smooth operation. Electrical heating allows to control and adjust the temperature inside the combustor's fluidised bed as desired.

The fluidised bed contains roughly 10 kg bed material corresponding to a bed height of around 500 mm.

The reactor can be fluidised with air, O<sub>2</sub>, CO<sub>2</sub>, CH<sub>4</sub>, steam or a mixture of these. There are six jets in the distributor for air, O<sub>2</sub>, CO<sub>2</sub> and two more jets for CH<sub>4</sub>. Every jet has four openings. Air, O<sub>2</sub> and CO<sub>2</sub> can be preheated through a two stage electrical pre-heater up to a maximum temperature of 900 °C.

Solid fuels are dosed through a double screw feeder system. The fuel container is slightly pressurised so as to avoid gas flow to the fuel container. The first screw feeder is used for dosing. The second screw works at higher "rpm"-s so as to pass all incoming fuel to the reactor. The rotational speed of both conveying screws is electronically controlled.

Downstream of the combustion chamber, the product gas is cleaned from particles by two cyclones (i.e. primary and protective) and a candle filter. Furthermore, the combustion flue gas is passed through a burner so as to make sure that no combustible species (e.g. during gasification) are released to the atmosphere. Finally, the gas passes a pressure control valve before it is vented to the atmosphere.

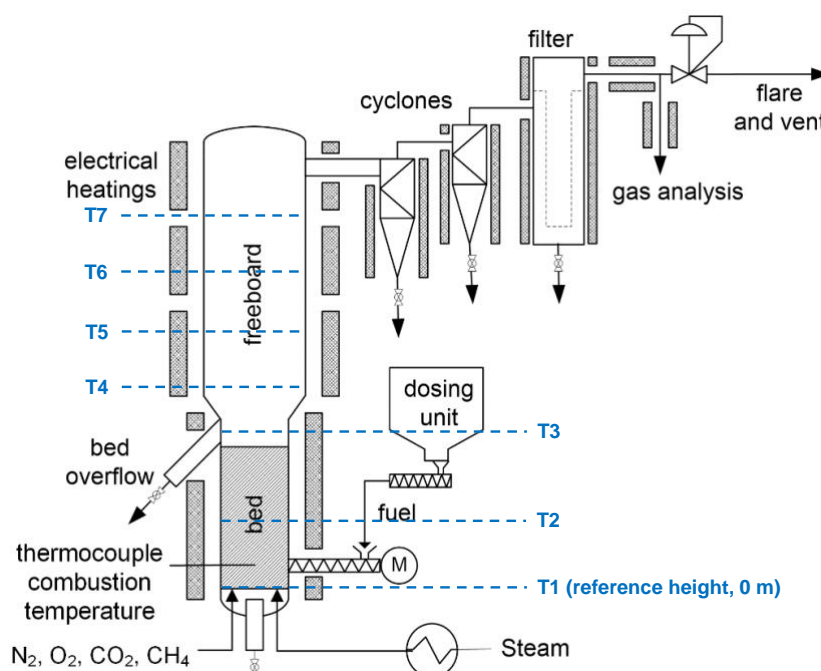


Figure 2. 20 kW bubbling fluidised bed combustion facility.

A slipstream of the product gas is extracted for gas measurements after the candle filter. Dry gas compositions are measured by non-dispersive infrared spectroscopy ( $\text{CO}_2$ ,  $\text{CO}$ ,  $\text{SO}_2$ ,  $\text{NO}_x$ ) and paramagnetism ( $\text{O}_2$ ). Furthermore, there is the possibility of connecting an FTIR system to measure additional flue gas species (e.g.  $\text{HCl}$ ).

The facility uses the commercial LabView® software for plant operation. All data (gas analysis, temperature and pressure data, etc.) are continuously displayed by the software and recorded and stored in excel files for subsequent evaluation.

## 3.2 Materials

### 3.2.1 Bed material

The lab-scale combustion tests introduced in this deliverable were completed using the commercial DORSILIT® silica sand as bed material (see Figure 3. Particle size distribution of the DORSILIT® silica sand and Table 1. Elemental analysis of the german DORSILIT® silica sand). Sand is considered to be inert within the process, as it will not modify the quality of the produced combustion gas. Hereby, quartz sand can be applied as a reference material for subsequent experiments involving other types (i.e. reactive) solid inventories, such as limestone.

**Table 1.** Elemental analysis of the german DORSILIT® silica sand.

	$\text{SiO}_2$ (wt%)	$\text{Al}_2\text{O}_3$ (wt%)	$\text{Fe}_2\text{O}_3$ (wt%)	$\text{K}_2\text{O}$ (wt%)	$\text{H}_2\text{O}$ (wt%)
DORSILIT®	95.0	2.5	0.04	2.3	0.16

Additionally, silica sand presents enhanced mechanical properties when it comes to attrition and fragmentation issues (when compared to limestone, for instance). This avoids the need of continuous fresh material supply to the system.

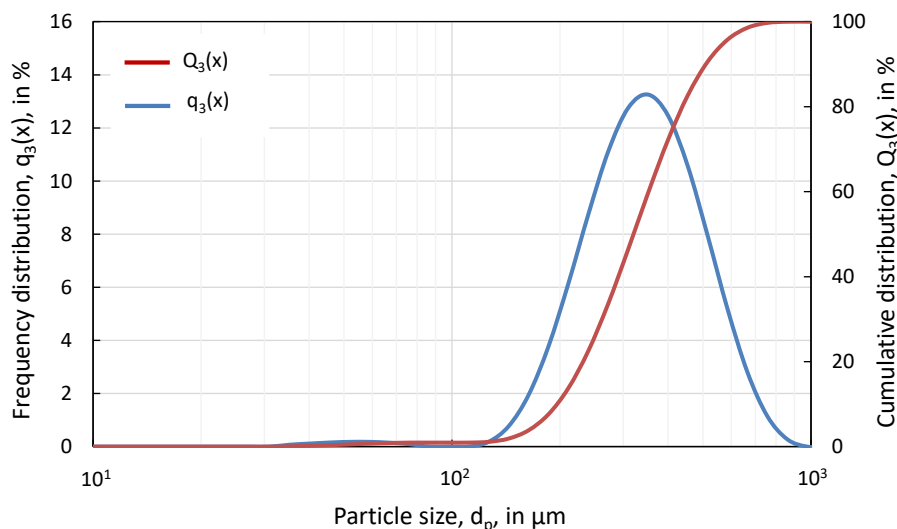


**Figure 3.** Particle size distribution of the DORSILIT® silica sand ( $d_{10} = 210 \mu\text{m}$ ;  $d_{50} = 320 \mu\text{m}$ ;  $d_{90} = 480 \mu\text{m}$ ).

### 3.2.2 Fuels

The first goal behind the combustion experiments at the 20 kW BFB combustion facility was to investigate the dosing of waste recovered fuels of different nature and conditioning degree.

In total four different solid recovered fuels (SRF) were selected for the dosing tests. These are described in Table 2. Description of the four SRFs selected for the and their properties (i.e. proximate and elemental analysis) are introduced in Table 3. Proximate and elemental analysis of the selected SRFs.

**Table 2.** Description of the four SRFs selected for the dosing tests.

Fuel	Provider	Bulk density	Nature	Conditioning
SBS-2	REMONDIS	≈ 70 kg/m <sup>3</sup>	Plastic-rich MSW (fluff)	Dried and crushed
CHEM	Chemnitz WIP	≈ 160 kg/m <sup>3</sup>	Organic-rich MSW (fluff)	Compacted (externally) and dried
SBS-1	REMONDIS	≈ 400 kg/m <sup>3</sup>	Lignin-rich MSW (compacted fluff)	Dried and preliminarily crushed, briquetted and manually crushed
ECO-P	ECO-Hispánica	≈ 800 kg/m <sup>3</sup>	Organic-rich MSW (pellet)	Steam treated and pelletised (externally)

**Table 3.** Proximate and elemental analysis of the selected SRFs.

	SBS-2	CHEM	SBS-1	ECO-P
Fixed Carbon (wt%, waf)	5.1	12.2	14.7	11.8
Volatiles (wt%, waf)	94.9	87.8	85.3	88.2
Moisture (wt%, a.r.)	1.5	53.0	1.5	10.0
Ash (wt%, wf)	6.5	33.8	11.8	20.7
Carbon (wt%, waf)	70.6	56.9	55.6	53.8
Hydrogen (wt%, waf)	10.2	7.4	7.1	8.7
Sulfur (wt%, waf)	0.2	0.6	0.3	0.4
Nitrogen (wt%, waf)	1.2	2.3	2.8	2.4
Oxygen (wt%, waf)	17.8	32.8	34.2	34.7
LCV (MJ/kg, a.r.)	29.5	5.8	18.7	14.3

According to Table 3. Proximate and elemental analysis of the selected SRFs, the SBS-1, CHEM and ECO-P fuels can be compared reasonably well against each other. This can actually be expected, due to the relative high organic content of these three SRFs. Some minor variations in this regard can be observed in the LCV, as a consequence of the different ash content of the fuels. On the contrary, SBS-2 presents a higher low calorific value compared with the SBS-1 (both provided by REMONDIS), as a result of the higher plastic content present in the fuel (note here the increased “C” and “H” concentrations).

The next section of this deliverable will focus therefore on assessing whether or not fuels of similar nature with different conditioning degree can influence the dosing quality in the 20 kW lab-scale facility combustor. A visual characterisation of the fuels is given in Figure 4. Visual characterisation of the different SRF types under study.



**Figure 4.** Visual characterisation of the different SRF types under study.

## 4 Cold dosing experiments

### 4.1 Methodology

The diverse origins and pre-treatments of waste derived fuels pose diverse technical challenges on the way these materials are dosed into combustion boilers. The dosing mechanism therefore constitutes a major aspect to look at when designing a waste incineration system.

In a preliminary phase of the oxy-fuel combustion experiments the dosing feasibility of each SRF type within the 20 kW dosing unit was investigated. The “cold” dosing tests were carried out with the experimental set-up depicted in

Figure 5. Detailed schematic of the 20 kW dosing system: whole (left), dosing device (right). In a first step, the fuel is charged into a downpipe which is directly connected to a feed hopper. The downpipe is equipped with two ball valves, which are necessary to decouple the pressurised vessel from the atmospheric pressure. Under normal operation, the fuel reaches gravimetrically the receiver tank. The mass flow rate of fuel is controlled by adjusting the rotational speed of the first (i.e. upper) screw conveyor. Then, the desired flow rate is directed gravimetrically through a free fall tube into a second (i.e. bottom) screw conveyor, which supplies fuel to the burner. The conveyed mass flow rate is calculated based on the change in the weighting signal registered by the dosing unit.

As for the cold experiments in this study, the free fall tube was decoupled from the bottom screw conveyor, allowing the material to be discharged into a collecting tray. The purpose here was twofold: i) to enable a better visualisation of the conveyed fuel mass flow rate; and ii) to avoid a laborious and unnecessary cleaning/clearing of the dosing unit after potential agglomeration issues.

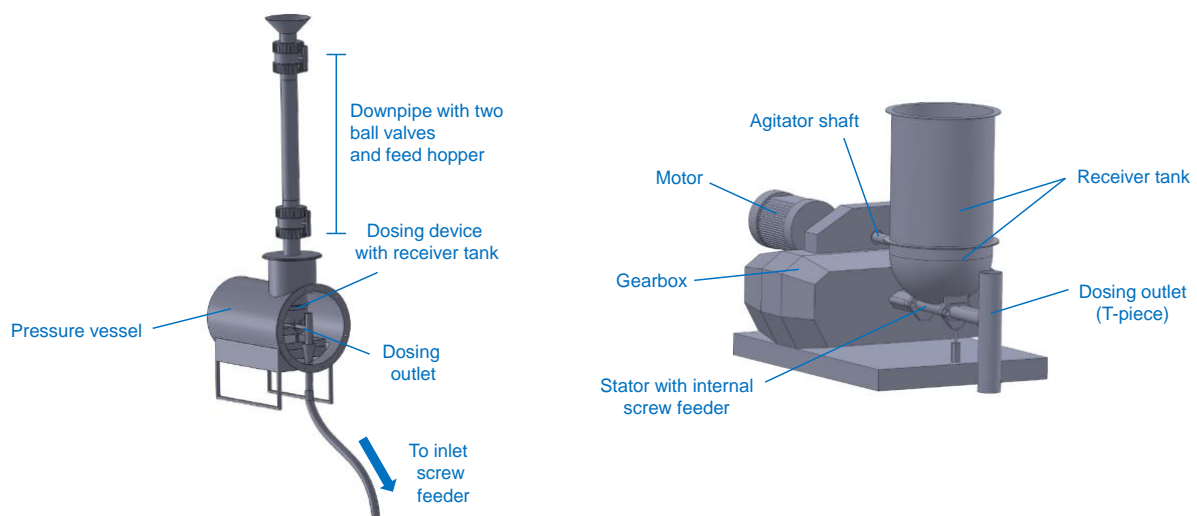


Figure 5. Detailed schematic of the 20 kW dosing system: whole (left), dosing device (right).

## 4.2 Results

### 4.2.1 SBS-2

The experimental investigation of cold waste dosing started with the SRF of lower bulk density, i.e. the SBS-2 provided by REMONDIS.



Figure 6. SBS-2 agglomeration in the pressure vessel (left), screw feeder (middle) and T-piece (right).

In a first phase of the test the fuel was charged into the downpipe connected to the hopper. The addition of large amounts of material led to agglomeration issues in the bottom part of the pipe, as a result of an increased pressure over the hopper. In view of this situation, it was decided to add the material in smaller amounts (i.e. approximately 1 kg per fuel loading). Once the receiver tank of the dosing unit got filled up, the rotational speed of the upper screw conveyor was set up to a medium speed (i.e. 500 rpm), without appreciable dosing rate signal though. At this point, the rotational speed was progressively increased up to the maximum value allowed by the device (i.e. 2000 rpm). Under these circumstances, the system software registered a stable mass flow rate signal. However, it was observed that no fuel was exiting the free fall tube, which suggested a fuel blockage issue somewhere in the dosing unit. As introduced in Figure 6. SBS-2 agglomeration in the pressure vessel (left), screw feeder (middle) and T-piece (right), it was observed that fuel got agglomerated in the first screw feeder, which led to clogging issues in the T-piece and thus to fuel backwater in the pressure vessel.

#### 4.2.2 CHEM

The experiences gained with SBS-2 showed that fuels of relative low bulk density could not be dosed effectively with the current system. Therefore, the next test considered a SRF of higher compaction density (i.e. the CHEM).

Following the methodology of the previous case, fuel was charged preliminarily into the downpipe. Although the material loading was improved with respect to the previous case, fuel dosing at medium-high rotational speeds (i.e. 1000 rpm) proved still to be irregular, and led finally again to clogging and backwater issues in the dosing unit.

This led the authors to the conclusion that the modest cross-sectional area of the 20 kW dosing system (i.e. screw feeders) was not able to cope with fuels of such low compacting degree. In view of this situation, three possible solutions could be suggested: i) a technical modification the whole fuel dosing system, ii) a conditioning (i.e. compacting) step for the already two tested SRFs and iii) a selection of additional SRFs with better dosing properties.

#### 4.2.3 SBS-1

The modification of the current dosing system would have been by far the most time-consuming solution to consider at the current project stage, since it would have altered (i.e. delayed) the completion of Task 3.2.1 significantly. In view of this situation, the authors decided to test the SBS-1 after prior conditioning (i.e. compacting).

Same as for SBS-2, SBS-1 was preliminarily crushed and dried. However, this SRF was subsequently briquetted (externally) and manually shredded to achieve a size fraction suitable to be dosed in the 20 kW feeding system. The bulk density of the final material achieved this way increased considerably with respect to the raw conditions (by about a factor of 5).

The dosing of cold SBS-1 proved to be successful even at low-medium low rotational speeds (i.e. 350 rpm), achieving mass flow rates close to the targeted values. Moreover, no clogging or agglomeration issues were registered downstream of the dosing unit. In view of these fact, it was decided to move on to the combustion experiments. These are introduced in the next section.

## 5 Combustion experiments

### 5.1 Air combustion tests

In view of the positive experience achieved with the cold dosing of SBS-1 it was decided to combust such fuel under air-firing conditions. This was carried out as a preliminary step to the oxy-fuel combustion tests, with a twofold objective: i) provide a comparison framework for the oxy-combustion experiments and ii) provide a first assessment of the SRF combustion behavior in FB systems.

#### 5.1.1 Experimental parameters

The experimental conditions defined for the air-combustion tests are summarised in Table 4. Experimental conditions defined for air-combustion experiments As can be observed, the tests aimed at investigating the influence of the combustion temperature over the ash behavior and the concentration of pollutants in the flue gas. As introduced in a previous section, the facility is preheated using electrical ceramic elements, which are accordingly turned off during the experiments.

The total inlet volumetric flow was accordingly adjusted in order to keep the gas superficial velocity constant within the three tests.

**Table 4.** Experimental conditions defined for air-combustion experiments.

Parameter	Case 1	Case 2	Case 3
	AIR-800	AIR-850	AIR-900
Reactor bed temperature, $\vartheta$ (°C)	800	850	900
Gas superficial velocity, $u$ (m/s)	0.55	0.55	0.55
Reactor bed inventory, $M_{\text{reactor}}$ (kg)	10	10	10
Inlet volumetric flow, $\dot{V}_{\text{in}}$ (m <sup>3</sup> /h, STP)	8.9	8.51	8.14
Air excess ratio, $n$	1.3	1.3	1.3

#### 5.1.2 Results

##### 5.1.2.1 SBS-1

The air-combustion experiments of SBS-1 began with Case 1 (i.e. 800 °C). Once the reactor reached the desired temperature set-point, the semi steady-state experiment could only be investigated for about 10 minutes, due to agglomeration issues observed in the fuel dosing unit. The average values of the main operation parameters recorded during the short semi-stable operational phase are introduced in Figure 7. Evolution of the main process parameters during the air-combustion of SBS-1

Observing the figure, one can note a slight excess in the air-flow rate during the semi-stable combustion phase, which indeed led to a certain dilution in the outlet CO<sub>2</sub> concentration. After the semi-stable phase, subsequent (partial) fuel congestion led to instable process conditions, which were investigated for another 8 minutes. This instable combustion behavior is well reflected by the

CO trend introduced in Figure 7, which peaked several times as a result of an inefficient mixture of fuel and oxygen.

In view of these circumstances, it was decided to conclude with the experiment and to proceed with the pelletised fuel (i.e. ECO-P) for the completion of the rest of the experimental plan.

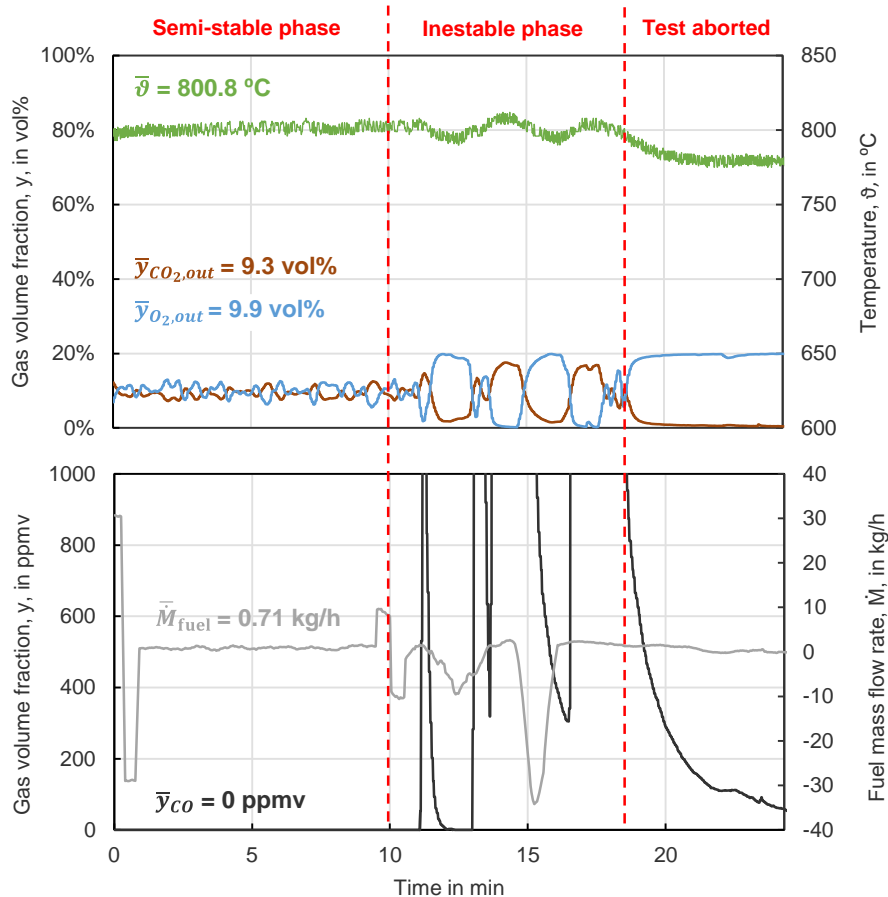


**Figure 7.** Evolution of the main process parameters during the air-combustion of SBS-1.

### 5.1.2.2 ECO-P

The conditioning of the available SRFs (i.e. SBS-1) proved not to solve the technical limitations observed in the 20 kW dosing system. At this point, it was decided to move on to a pelletised SRF of considerable higher bulk density (i.e. ECO-P).

The usage of ECO-P did not show any dosing problems. Air combustion experiments with an excess ratio of approximately 1.3 were completed at 800 °C, 850 °C and 900 °C. The experiments were investigated for operational times longer than one hour each under stable conditions (see Figure 8. Temperature and pressure profiles, gas concentrations and fuel flow rate of the combustor under air-firing conditions). As indicated by the reactor's differential pressure evolution along with the three air-combustion experiments, no bed agglomeration and/or fuel congestion issues were observed. The switch between experimental points proved to be smooth and uniform, as shown by the gas concentration trends (i.e. CO<sub>2</sub> and O<sub>2</sub>) and temperature profile depicted in the figure. Further parameters of interest such as SO<sub>2</sub> and CO volume fractions evolved uniformly, and averaged by 3 and 93 ppm, respectively. Please note that these average values consider the stable phase achieved

within the three experiments, and not the transition phases between them. The gas superficial velocity ( $u_{\text{reactor}}$ ) was kept constant at 0.55 m/s and the reactor bed inventory ( $M_{\text{reactor}}$ ) averaged by 9.7 kg.

The evaluation of the obtained results is introduced in Table 5. Comparison between the air-combustion results obtained in the 20 kW facility and those obtained through balance equations and process simulation (in bold), together with some additional calculations and simulations which provide a comparison framework for the plant data. These are: i) balance equations derived from a fundamental combustion calculations, assuming full combustion conditions and ii) simulation results calculated using a simplified oxy-fuel combustion model by Aspen Plus. A detailed description of i) and ii) is introduced in the Annex included at the end of this deliverable.

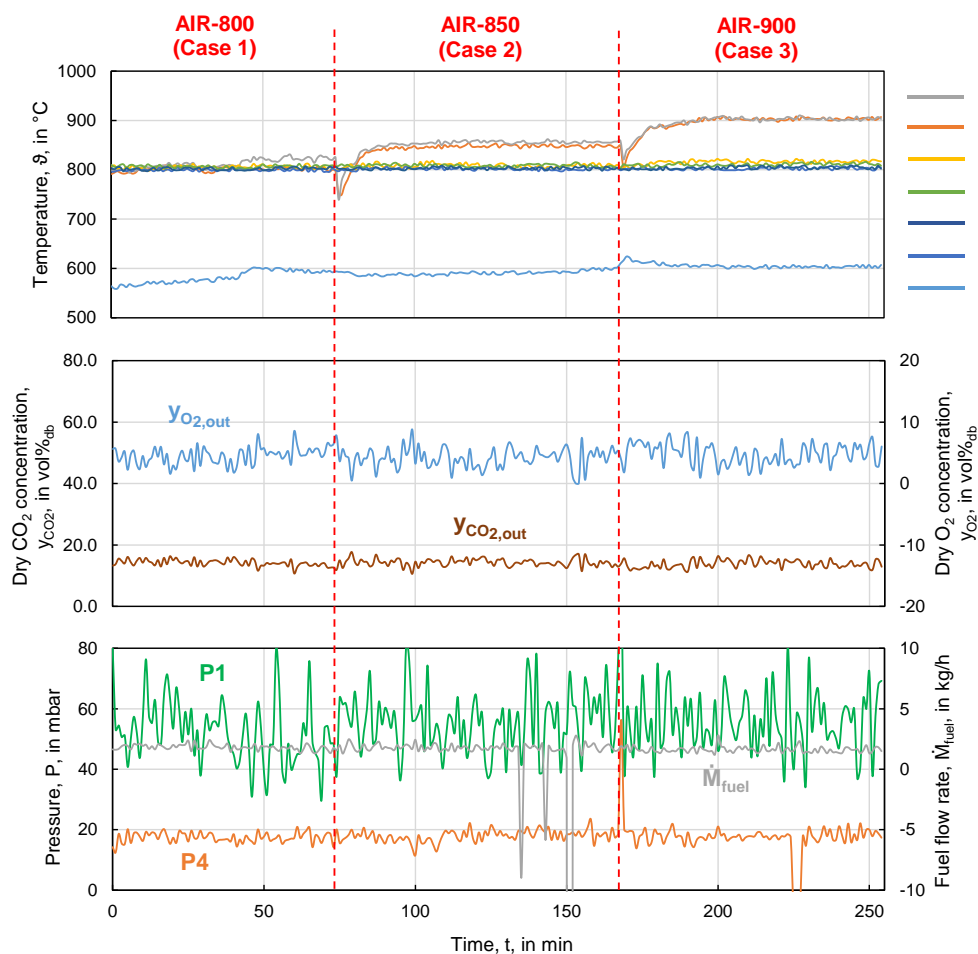


**Figure 8.** Temperature and pressure profiles, gas concentrations and fuel flow rate of the combustor under air-firing conditions.

**Table 5.** Comparison between the air-combustion results obtained in the 20 kW facility and those obtained through balance equations and process simulation (in bold).

Parameter	Experimental data			Balance equations			Aspen Plus® Simulation		
	800 °C	850 °C	900 °C	800 °C	850 °C	900 °C	800 °C	850 °C	900 °C
$\vartheta$ (°C)	801.5	847.1	<b>901.6</b>	n/a	n/a	<b>n/a</b>	801.5	847.1	901.6

$\dot{M}_{\text{fuel}}$ (kg/h)	1.84	1.76	1.66	1.84	1.76	1.66	1.84	1.76	1.66
$M_{\text{reactor}}$ (kg)	9.5	9.8	9.8	n/a	n/a	n/a	n/a	n/a	n/a
$\dot{V}_{\text{in}}$ (m <sup>3</sup> /h, STP)	8.88	8.49	8.13	8.88	8.49	8.13	8.88	8.49	8.13
$\dot{V}_{\text{out}}$ (m <sup>3</sup> /h, STP)	n/a	n/a	n/a	9.6	9.2	8.6	9.9	9.4	9.0
$y_{\text{CO}_2,\text{out}}$ (vol% <sub>db</sub> )	14.1	14.3	14.1	14.5	14.5	14.5	14.1	15.1	14.9
$y_{\text{O}_2,\text{out}}$ (vol% <sub>db</sub> )	4.5	4.2	4.4	4.9	4.9	4.9	3.3	3.5	3.8
$y_{\text{N}_2,\text{out}}$ (vol% <sub>db</sub> )	81.3	81.5	81.5	80.5	80.5	80.5	82.4	81.2	81.2
$y_{\text{H}_2\text{O},\text{out}}$ (vol%)	n/a	n/a	n/a	11.3	11.3	11.3	11.6	11.6	11.5
$y_{\text{CO},\text{out}}$ (ppmv <sub>db</sub> )	63	157	58	0	0	0	0	0	0
$y_{\text{SO}_2,\text{out}}$ (ppmv <sub>db</sub> )	2	3	3	642	642	642	383	431	436

As introduced in Table 5. Comparison between the air-combustion results obtained in the 20 kW facility and those obtained through balance equations and process simulation (in bold), the calculations obtained from balance equations and process simulations correlate reasonably well with the experimental plant data. Furthermore, these two validation tools provide additional estimations which cannot be obtained from the facility, i.e. total outlet gas volumetric flow and humidity content of the flue gas. Some minor deviations can be observed in some trace gas species, such as CO and SO<sub>2</sub>. As for CO, this can be related to the fact of measuring close to the lower detection limit of the gas analyser (measuring range: 0-5000 ppmv), which indeed can lead to inaccurate or misleading values. Moreover, the observed low SO<sub>2</sub> concentrations can be related to calcium deposits from previous experiments downstream the combustor unit. This can occur when limestone is used as bed material during combustion or gasification experiments. In such conditions, the calcium deposits may interact with the SO<sub>2</sub> from the flue gas, capturing it in form of sulphate.

A relevant part of the process evaluation comprises the ash analysis of the sorbent bed material. Indeed, it is well known that certain ash compounds interact with the inert material of the fluidised bed, whose reactions lead to the formation of sticky coatings around bed particles. This cause them to adhere to each other, forming agglomerates that eventually inhibit further fluidisation.

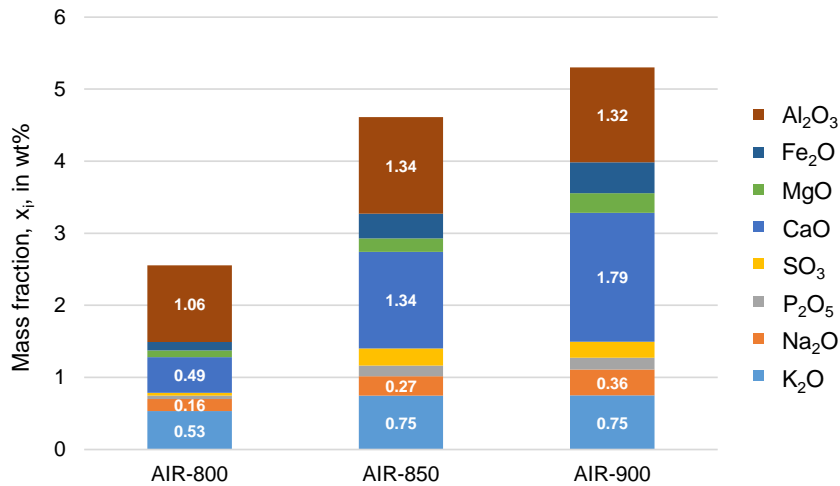


**Figure 9.** Mass fraction of the main ash components in the reactor solids sampled during the air-combustion experiments (rest fraction: SiO<sub>2</sub>).

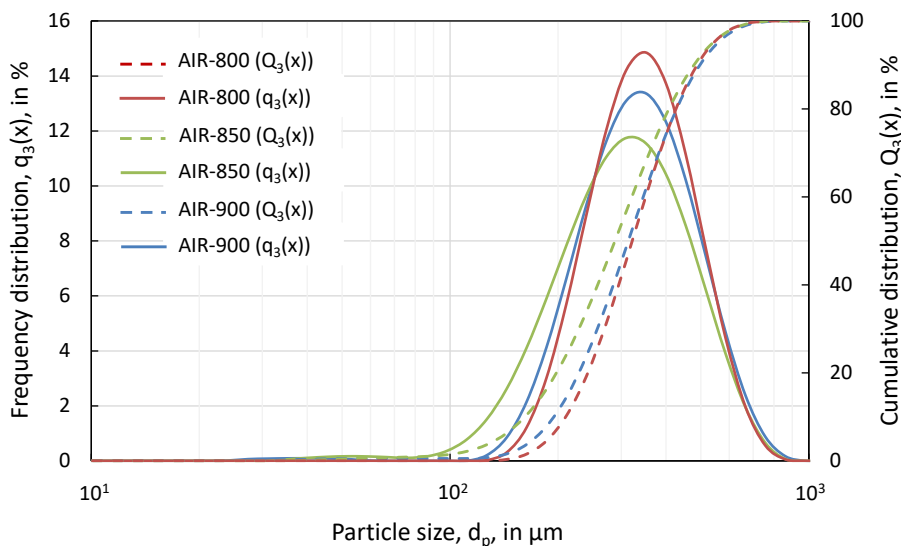


**Figure 10.** Particle size distribution of the reactor solids sampled during the air-combustion experiments.

Figure 9. Mass fraction of the main ash components in the reactor solids sampled during the air-combustion experiments (rest fraction: SiO<sub>2</sub>) introduces the composition of the bottom ash sampled from each air-combustion experiment investigated in the 20 kW facility. Generally, the mass fraction of each ash component increased along with the experimental time and combustion temperature, particularly from 800 °C to 850 °C. Some did it to a larger extent (e.g. CaO), while some others did only increase slightly (e.g. Al<sub>2</sub>O<sub>3</sub>). It must be noted, that the Al<sub>2</sub>O<sub>3</sub> found in the ash analysis might belong to the Al<sub>2</sub>O<sub>3</sub> originally found in the silica sand. As for the alkali species, the content of Na<sub>2</sub>O in the ash increased more significantly than for K<sub>2</sub>O.

As for the particle size distribution (PSD) of the bed solids (see Figure 10. Particle size distribution of the reactor solids sampled during the air-combustion experiments), no major differences can be observed in the mentioned temperature range.

## 5.2 Oxy-fuel combustion tests

The successful investigation of the preliminary air-combustion of ECO-P led to a first assessment of the fuel in terms of ash behaviour (e.g. agglomeration tendency, bottom ash composition) and the concentration of pollutants in the flue gas. The results and experience gained in these experiments were used to choose promising experimental conditions for the oxy-fuel combustion tests, so as to reduce the risk of technical problems.

### 5.2.1 Experimental parameters

The experimental conditions defined for the three oxy-fuel combustion tests under study are summarised in Table 6. Experimental conditions defined for the oxy-fuel combustion experiments

**Table 6.** Experimental conditions defined for the oxy-fuel combustion experiments.

Parameter	Case 4: OXY-21	Case 5: OXY-30	Case 6: OXY-40
Reactor bed temperature, $\vartheta$ (°C)	850	850	850
Gas superficial velocity, $u$ (m/s)	0.55	0.55	0.55
Reactor bed inventory, $M_{\text{reactor}}$ (kg)	10	10	10
Inlet volumetric flow, $\dot{V}_{\text{in}}$ (m <sup>3</sup> /h, STP)	8.51	8.51	8.51
Inlet dry oxygen concentration, $y_{\text{O}_2,\text{in}}$ (vol% <sub>db</sub> )	21	30	40
Inlet dry oxygen concentration, $y_{\text{CO}_2,\text{in}}$ (vol% <sub>db</sub> )	71.4	62.4	52.4
Inlet dry oxygen concentration, $y_{\text{N}_2,\text{in}}$ (vol% <sub>db</sub> )	7.6	7.6	7.6

As can be observed, the tests aimed at investigating the influence of different inlet oxygen concentrations over the process performance (i.e. ash behavior and concentration of pollutants in the flue gas). The combustion temperature in this case was kept unvaried, together with the total inlet volumetric flow (and thus the gas superficial velocity). The oxygen volumetric flow was balanced with CO<sub>2</sub> in order to simulate a realistic recycled oxy-fuel flue gas stream. Additionally, some nitrogen was required to flush the pressure transducers of the lab-scale facility.

### 5.2.2 Results

#### 5.2.2.1 ECO-P

The evolution of the main combustion parameters during the oxy-fuel tests is introduced in Figure 11. Temperature and pressure profiles, gas concentrations and fuel flow rate of the combustor under oxy-fuel firing conditions. As can be seen in the figure, each test was investigated at least one hour under stable process conditions. The temperature profile of the reactor in this case was uniform and averaged by 850 °C along with the whole combustor height. As for Case 6 (OXY-40) the temperature in the windbox (i.e. T1) decreased significantly during the experiment. This cooling down procedure was applied so as to maintain the set-point temperature within the reactor (i.e. 850 °C), which

otherwise would have increased considerably as a result of the high flame temperatures achieved with such high inlet oxygen levels. Please note that the facility does not offer the possibility of recirculating the combustion flue gas. As for the outlet  $\text{CO}_2$  and  $\text{O}_2$  concentrations achieved along with the three experiments, these averaged by 83.9 vol%<sub>db</sub> and 6.9 vol%<sub>db</sub>, respectively. Please note here the dilution effect posed by the nitrogen, required for the flushing of the pressure transducers (by about 9 vol%<sub>db</sub>). Additionally, the stable evolution of the differential reactor pressure (i.e. P1-P4) indicates that no agglomeration effects were observed in this case either. Gas polluting species such as  $\text{SO}_2$  and CO (not depicted in the figure) averaged by 4 ppmv<sub>db</sub> and 91 ppmv<sub>db</sub>, respectively. The gas superficial velocity ( $u_{\text{reactor}}$ ) was kept constant at 0.55 m/s and the reactor bed inventory ( $M_{\text{reactor}}$ ) averaged by 10.2 kg.

Same as for the air-combustion experiments, the plant data in this case was validated against the results obtained from the balance equations and the simulation model (see Table 7. Comparison between the oxy-fuel combustion results obtained in the 20 kW facility and those obtained through balance equations and process simulation (in bold).).

Generally, the plant data can be compared well with the equation and model results. The outlet dry and nitrogen-free gas volume fractions ( $\text{CO}_2$  and  $\text{O}_2$ ) are similar in all three compared scenarios, as well as the calculated total outlet flue gas volumetric flow. Minor differences can be observed in the humidity content of the flue gas, for instance. The water fraction calculated through the balance equations is slightly higher than the one obtained from process simulation (by about 3 percentage points). As for CO and  $\text{SO}_2$ , the same effect as in air-combustion mode can be observed. Considering the relatively high excess of oxygen (> 6 vol%<sub>db</sub>) the presence of CO in the flue gas is questionable. Taking into account the wide CO concentration range of the gas analyser (i.e. 0 – 5000 ppmv), the low CO emission values recorded in the facility are close to the lower detection limit of the device (i.e. 0 ppmv), which in turn can introduce an error in such low measurement range. As for  $\text{SO}_2$ , the low emission values detected by the analyser might be linked once again to CaO depositions downstream the reactor (i.e. gas ducts, candle filter, etc.) from previous experiments, which even if in relatively low amounts, might capture the  $\text{SO}_2$  originated from the combustion process.

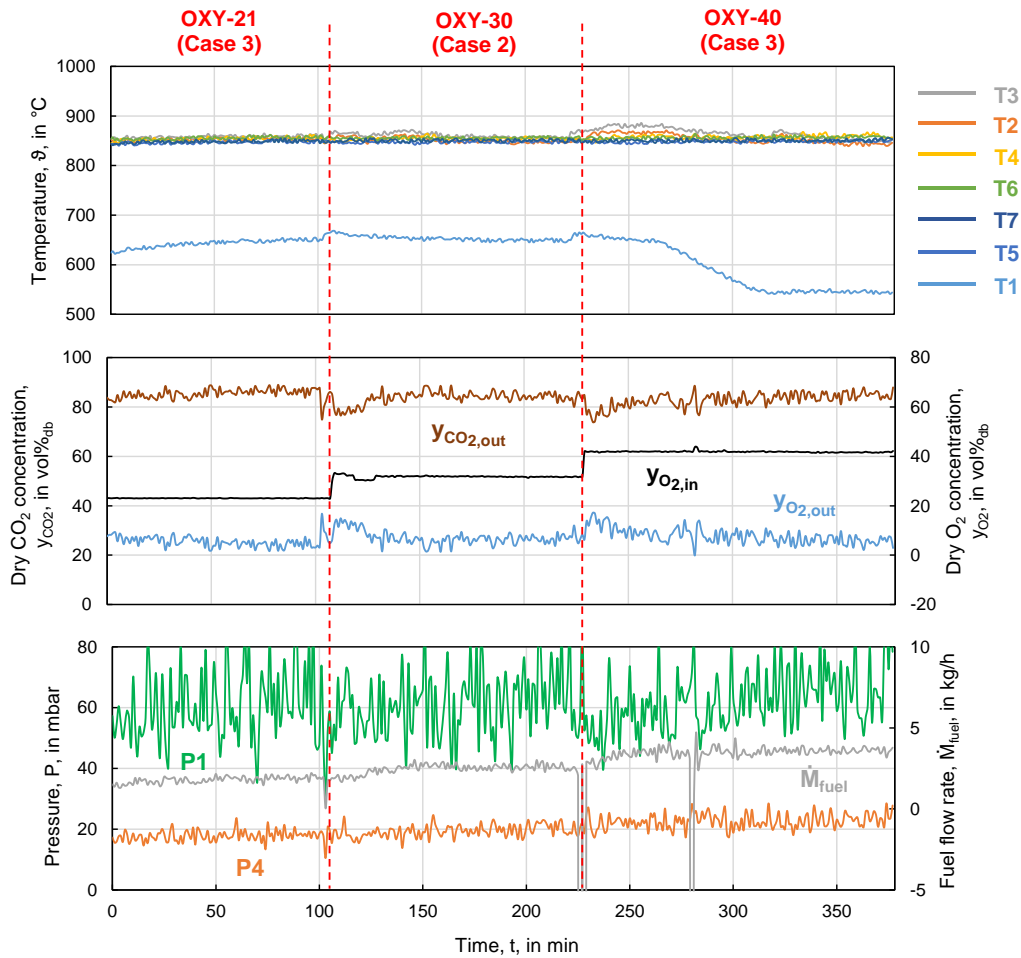


**Figure 11.** Temperature and pressure profiles, gas concentrations and fuel flow rate of the combustor under oxy-fuel firing conditions.

**Table 7.** Comparison between the oxy-fuel combustion results obtained in the 20 kW facility and those obtained through balance equations and process simulation (in bold). \*Given in a nitrogen-free basis, according to representative oxy-fuel combustion conditions.

Parameter	Experimental data			Balance equations			Aspen Plus® Simulation		
	OXY-21	OXY-30	OXY-40	OXY-21	OXY-30	OXY-40	OXY-21	OXY-30	OXY-40
$\vartheta$ (°C)	852.2	851.1	<b>850.1</b>	n/a	n/a	n/a	852.2	851.1	850.1
$\dot{M}_{fuel}$ (kg/h)	1.78	2.57	<b>3.60</b>	1.78	2.57	3.60	1.78	2.57	3.60
$M_{reactor}$ (kg)	10.6	10.2	<b>10.1</b>	n/a	n/a	n/a	n/a	n/a	n/a
$\dot{V}_{in}$ (m <sup>3</sup> /h, STP)	8.49	8.51	<b>8.50</b>	8.49	8.51	8.50	8.49	8.51	8.50
$\dot{V}_{out}$ (m <sup>3</sup> /h, STP)	n/a	n/a	<b>n/a</b>	<b>9.7</b>	<b>10.3</b>	<b>11.0</b>	9.5	9.9	10.4
$y_{CO_2,out}$ (vol% <sub>db</sub> )*	93.9	92.8	<b>91.3</b>	<b>93.5</b>	<b>92.2</b>	<b>92.1</b>	93.4	91.8	91.4

$y_{O_2,out}$ (vol% <sub>db</sub> )*	6.0	7.2	8.7	6.5	7.8	7.8	6.4	7.9	8.3
$y_{H_2O,out}$ (vol%)	n/a	n/a	n/a	14.4	19.6	25.2	11.8	16.2	21.3
$y_{CO,out}$ (ppmv <sub>db</sub> )*	43	91	41	0	0	0	0	0	0
$y_{SO_2,out}$ (ppmv <sub>db</sub> )*	4	4	4	533	773	1087	469	674	949

The elemental analysis comparison of the samples taken in the reactor and in the secondary (i.e. protective) cyclone is introduced in Figure 12. Elemental composition (in wt%) of the solid inventory sampled from the oxy-fuel combustion experiments (rest fraction: SiO<sub>2</sub>) and Figure 13. Elemental composition (in wt%) of the fly ash sampled from the oxy-fuel combustion experiments (rest fraction: SiO<sub>2</sub>), respectively.

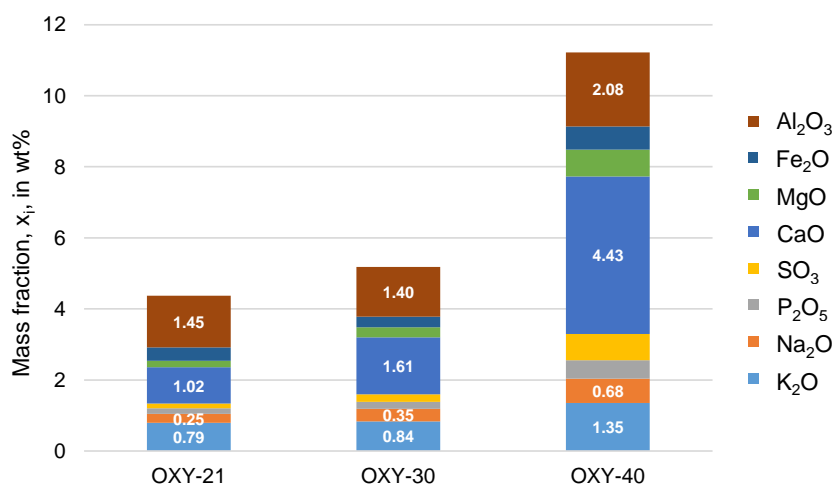


**Figure 12.** Elemental composition (in wt%) of the solid inventory sampled from the oxy-fuel combustion experiments (rest fraction: SiO<sub>2</sub>)

As the ash elemental analysis of the bed material sampled during OXY-30 can be compared to the AIR-850 case fairly well, operation under higher oxy-fuel levels (i.e. 40 vol%) seems to increase ash deposition in the fluidised bed. This effect has been already recognised by some authors [1,15]. The same behavior is also reflected in the PSD analysis of the bottom ash during the OXY-40 case (see Figure 14. Particle size distribution of the solid bed material sampled during the oxy-fuel combustion experiments.), which is significantly coarser than in the two other oxy-fuel cases (i.e. OXY-21 and OXY-30), as a result of the higher ash availability in the bed.

On the other hand, concerning the elemental composition of the fly ash sampled during the three investigated oxy-fuel experiments, no major differences can be regarded either in the total amount of ash or in the elemental analysis of the solids. As for the PSD (see Figure 15. Particle size distribution of the fly ash sampled during the oxy-fuel combustion experiments.), the fine ash particles collected in the protective cyclone suggest certain agglomeration behavior compared with the two previous oxy-fuel cases (i.e. OXY-21 and OXY-30). This correlates well to the behavior observed in the bottom ash PSD during OXY-40, where the coarser fraction was also dominating.

Therefore, it seems that the ash formation and deposition behavior during oxy-fuel combustion comprises a major aspects to look at when operating particularly at high  $O_2$  concentrations, due to the technical limitations this effect can pose on process operation.

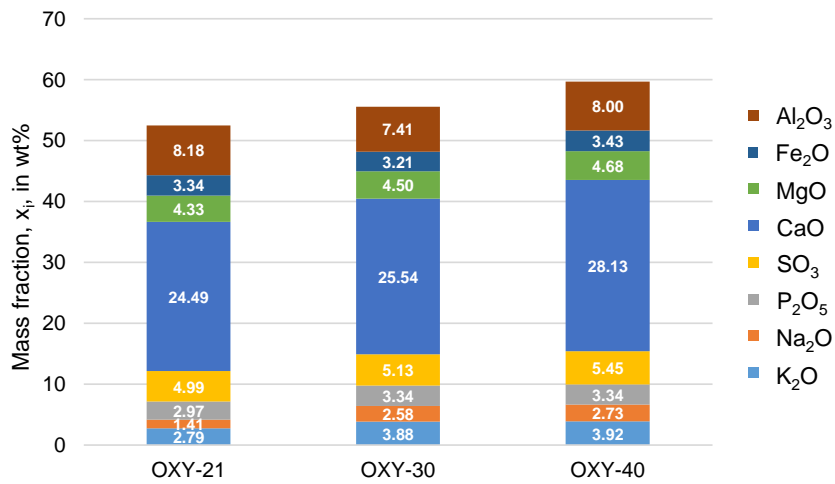


**Figure 13.** Elemental composition (in wt%) of the fly ash sampled from the oxy-fuel combustion experiments (rest fraction:  $SiO_2$ )

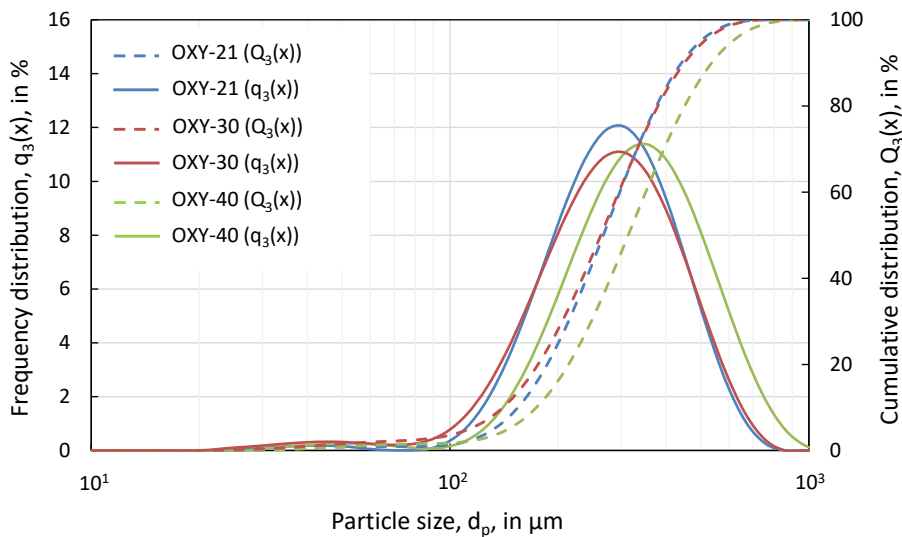


**Figure 14.** Particle size distribution of the solid bed material sampled during the oxy-fuel combustion experiments.

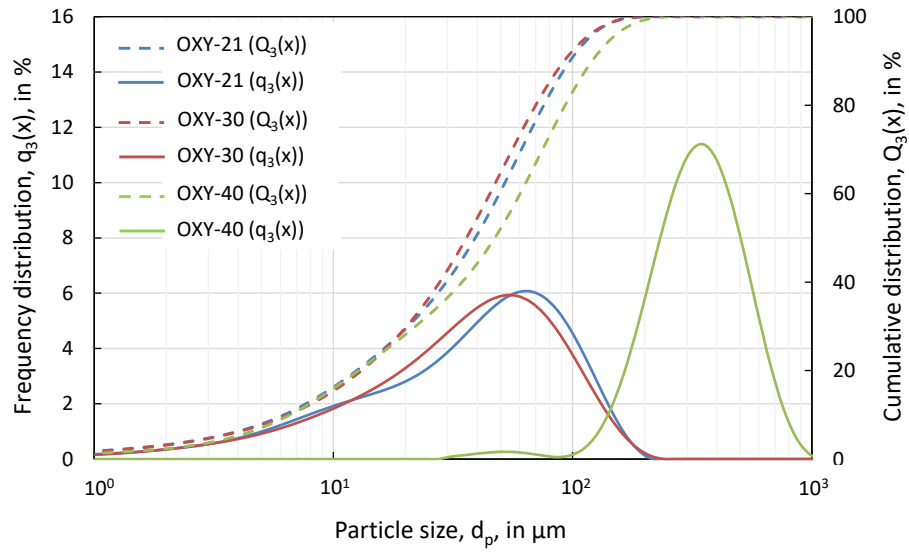


**Figure 15.** Particle size distribution of the fly ash sampled during the oxy-fuel combustion experiments.

## 6 Conclusions and Outlook

In the present study, a preliminary assessment of solid recovered fuel (SRF) combustion has been performed at the 20 kW lab-scale BFB combustor of the University of Stuttgart.

Cold dosing experiments of four different fuels (i.e. SBS-2, CHEM, SBS-1 and ECO-P) revealed that only fuels with sufficient bulk density and compacting degree (i.e. SBS-1 and ECO-P) were suitable for efficient dosing with the current dosing unit. Even if SBS-1 could be successfully dosed and air-combusted for a few hours, the fuel finally led to agglomeration and clogging issues. This led to the decision of utilising a pelletised and thus more compact SRF (i.e. ECO-P) more the completion of the air and oxy-fuel experiments.

Cold dosing of ECO-P was completed without any technical inconveniences. Air combustion experiments were investigated at different reactor temperatures: 800 °C, 850 °C and 900 °C. The combustion behavior proved to be smooth and uniform, without technical limitations imposed by bed agglomeration. The data obtained from the pilot facility proved to be comparable to the calculations obtained from combustion balance equations and process simulations, assuring the validity of the results. The bottom ash concentration proved to increase together with the reactor temperature, but the PSD of such solids revealed no major variations in the size trend along with the reactor temperature. After successful combustion investigations under air-firing conditions, three oxy-fuel experiments were subsequently studied: OXY-21, OXY-30 and OXY-40. Here as well, a smooth and consistent combustion behavior could be demonstrated. Once again, plant data proved to match the balance equations and simulation calculations fairly well. The analysis of the bed material indicated a significant increase in the ash content at relatively high O<sub>2</sub> concentrations (i.e. 40 vol%<sub>db</sub>), which correlates with some literature works. Moreover, the PSD of such solids suggested certain bed agglomeration behavior, which could have been originated as a consequence of the increased ash concentration in the bed. The same behavior was found in the solids sampled in the protective cyclone (i.e. fly ash). Although this effect did not lead to technical limitations in the current study, it may be worth investigating in future works, particularly in those involving high oxy-fuel levels and long experimental demonstrations.

The results and experience gained in the lab-scale BFB combustor will serve to choose promising experimental conditions for demonstration at the 200 kW CFB pilot facility combustor. Experiments in this regard are scheduled by the end of 2020.

### Acknowledgements

The authors acknowledge the financial support by the Federal Ministry for Economic Affairs and Energy of Germany in the project NEWEST-CCUS (project number 299683).

The authors would also like to thank the academic colleagues Felix Mangold and Tim Seitz for their experimental support, and W. Ross and his team of IFK's "Laboratory for Fuels, Ashes and Slag" for supporting this work with lab analyses of fuels and sorbents.

## References

- [1] Al-Qayim K, Nimmo W, Hughe KJ, Pourkashanian M. Effect of oxy-fuel combustion on ash deposition of pulverized wood pellets. *Biofuel Res. J.* 2019;6(1):927–36. <https://doi.org/10.18331/BRJ2019.6.1.4>.
- [2] Aspen Technology, Inc. ASPEN PLUS® User Guide. Version 10.2.
- [3] Aspen Technology, Inc. Getting Started Modeling Processes with Solids. V8.4.
- [4] Clerens P, Thuau A. The Role of Waste-to-Energy (WtE) in the EU's Long-Term Greenhouse Gas Emissions Reduction Strategy 2018.
- [5] Ditaranto M, Becidan M, Stuen J. Opportunities for CO<sub>2</sub> Capture in the Waste-to-Energy Sector 2019.
- [6] EUROPEAN COMMISSION. The role of waste-to-energy in the circular economy. Brussels; 2017.
- [7] Guo J, Zhang T, Huang X, Luo W, Hu F, Luo Z et al. Oxy-Fuel Combustion Characteristics of Pulverized Coal in a 3 MW Pilot-Scale Furnace. *Energy Fuels* 2018;32(10):10522–9. <https://doi.org/10.1021/acs.energyfuels.8b02275>.
- [8] Hrdlicka J, Skopec P, Opatril J, Dlouhy T. Oxyfuel Combustion in a Bubbling Fluidized Bed Combustor. *Energy Procedia* 2016;2016:116–23. <https://doi.org/10.1016/j.egypro.2016.01.012>.
- [9] Kiriishi K, Fujimine T, Hayakawa A. High Efficiency Furnace with Oxy-Fuel Combustion and Zero-Emission by CO<sub>2</sub> Recovery 2009.
- [10] Kosowska-Golachowska M, Luckosb A, Pelkaa P, Klosa K, Musiala T. Experimental research of the oxy-fuel combustion in a circulating fluidized bed 2011.
- [11] Liu Q, Shi Y, Zhong W, Yu A. Co-firing of coal and biomass in oxy-fuel fluidized bed for CO<sub>2</sub> capture: A review of recent advances. *Chinese Journal of Chemical Engineering* 2019;27(10):2261–72. <https://doi.org/10.1016/j.cjche.2019.07.013>.
- [12] Scarlat N, Fahl F, Dallemand J-F. Status and Opportunities for Energy Recovery from Municipal Solid Waste in Europe. *Waste Biomass Valor* 2019;10(9):2425–44. <https://doi.org/10.1007/s12649-018-0297-7>.
- [13] Sher F, Pans MA, Sun C, Snape C, Liu H. Oxy-fuel combustion study of biomass fuels in a 20 kW<sub>th</sub> fluidized bed combustor. *Fuel* 2018;215:778–86. <https://doi.org/10.1016/j.fuel.2017.11.039>.
- [14] Wienchol P, Szlęk A, Ditaranto M. Waste-to-energy technology integrated with carbon capture. Challenges and opportunities. *Energy* 2020;198:117352. <https://doi.org/10.1016/j.energy.2020.117352>.
- [15] Wu J, Wang Y, Han J, Li X, Yu D, Xu M et al. Ash Formation and Deposition in Oxy-fuel Combustion of Rice Husk, Coal, and Their Blend with 70% Inlet O<sub>2</sub>. *Energy Fuels* 2020;34(1):890–9. <https://doi.org/10.1021/acs.energyfuels.9b03129>.

## Annex

### A1) Elementary (stoichiometric) combustion calculations

The following section has been extracted from the Chapter 3 of the Lecture “Firing Systems and Flue Gas Cleaning, 2019/2020” held at the University of Stuttgart.

A complete combustion comprises the full combustion of all the carbon to CO<sub>2</sub>, all the hydrogen to H<sub>2</sub>O and all the sulphur to SO<sub>2</sub>:



Therefore, the basis for the calculation is an ultimate fuel analysis. The fuel mass balance results in:

$$\gamma_C + \gamma_H + \gamma_S + \gamma_O + \gamma_N + \gamma_{H_2O} + \gamma_A = 1 \quad (4)$$

When considering an stoichiometric combustion calculation there are the following relations between specific oxygen- and air requirement in accordance with the combustion reactions of the pure components C, H and S:

$$\mu_{O_2o} = \left( \frac{\gamma_C}{M_C} + \frac{\gamma_H}{2 \cdot M_{H_2}} + \frac{\gamma_S}{M_S} - \frac{\gamma_O}{M_{O_2}} \right) \cdot M_{O_2} \quad (5)$$

$$\mu_{LoT} = \frac{\mu_{O_2o}}{x_{O_2LT}} \quad (6)$$

$$\mu_{Lo} = \mu_{LoT} \cdot (1 + x_{H_2OLT}) \quad (7)$$

For the combustion with air we use the physical properties summarised in DIN 1871. The mass fractions are given as follows:

$x_{N_2LT}$	= 0.755425	Nitrogen	
$x_{ArLT}$	= 0.012653	Argon (with neon)	
$x_{CO_2LT}$	= 0.000505	Carbon dioxide	(8)
$x_{O_2LT}$	= 0.231417	Oxygen	

And the specific flue gas components can then be calculated as:

$$\mu_{CO_2o} = \frac{M_{CO_2}}{M_C} \cdot \gamma_C + \mu_{LoT} \cdot x_{CO_2LT} \quad (9)$$

$$\mu_{SO_2o} = \frac{M_{SO_2}}{M_S} \cdot \gamma_S \quad (10)$$

$$\mu_{N_2o} = \gamma_N + \mu_{LoT} \cdot x_{N_2LT} \quad (11)$$

$$\mu_{ArO} = \mu_{LoT} \cdot x_{ArLT} \quad (12)$$

$$\mu_{H_2Oo} = \frac{M_{H_2O}}{M_{H_2}} \cdot \gamma_H + \gamma_{H_2O} + \mu_{LoT} \cdot x_{H_2OLT} \quad (13)$$

And the specific flue gas amount:

$$\mu_{GoT} = \mu_{CO_2o} + \mu_{SO_2o} + \mu_{N_2o} + \mu_{Aro} \quad (14)$$

$$\mu_{Go} = \mu_{GoT} + \mu_{H_2Oo} \quad (15)$$

Furthermore, the mass balance results in:

$$\mu_{Go} = \mu_{Lo} + 1 - \gamma_A \quad (16)$$

When combusting with excess air ( $n > 1$ , where  $n$  = actual air requirement / stoichiometric air requirement) we obtain:

$$\Delta\mu_{LT} = (n-1) \cdot \mu_{LoT} \quad (17)$$

$$\mu_{LT} = \mu_{LoT} + \Delta\mu_{LT} \quad (18)$$

$$\mu_L = \mu_{Lo} + \Delta\mu_{LT} (1 + x_{H_2OLT}) \quad (19)$$

The specific flue gas components for combustion with excess air can be determined then by analogous supplement of the equations (9), (11) to (13) with  $\Delta\mu_{LT}$ . Additionally, a correlation for the specific concentration of oxygen in the flue gas has to be added. We obtain then:

$$\mu_{CO_2} = \mu_{CO_2o} + \Delta\mu_{LT} \cdot x_{CO_2LT} \quad (20)$$

$$\mu_{SO_2} = const. \quad (21)$$

$$\mu_{N_2} = \mu_{N_2o} + \Delta\mu_{LT} \cdot x_{N_2LT} \quad (22)$$

$$\mu_{Ar} = \mu_{Aro} + \Delta\mu_{LT} \cdot x_{ArLT} \quad (23)$$

$$\mu_{O_2} = \Delta\mu_{LT} \cdot x_{O_2LT} \quad (24)$$

$$\mu_{H_2O} = \mu_{H_2Oo} + \Delta\mu_{LT} \cdot x_{H_2OLT} \quad (25)$$

The following equations are valid for the calculation of the specific flue gas quantities by combustion with excess air:

$$\mu_{GT} = \mu_{GoT} + \Delta\mu_{LT} \quad (26)$$

$$\mu_G = \mu_{Go} + \Delta\mu_{LT} \cdot (1 + x_{H_2OLT}) \quad (27)$$

The mass fractions of  $x_{iT}$  (dry) and  $x_i$  (wet) can now be determined with the knowledge of the six single components  $CO_2$ ,  $SO_2$ ,  $N_2$ ,  $Ar$ ,  $O_2$  and  $H_2O$  to:

$$x_{iT} = \frac{\mu_i}{\mu_{GT}} \quad (28)$$

$$x_i = \frac{\mu_i}{\mu_G} \quad (29)$$

And the specific flue gas volume and the volume fractions of single components in the flue gas can be then calculated as follows:

$$\rho_{ni} = \frac{M_i}{V_{mni}} \quad (30)$$

$$y_k = \frac{\frac{x_k}{\rho_{nk}}}{\sum_i \frac{x_i}{\rho_{ni}}} \quad (31)$$

$$\bar{\rho}_n = \sum y_i \cdot \rho_{ni} \quad (32)$$

The corresponding equations for the combustion with a different oxygen carrier (e.g. oxy-fuel combustion with flue gas recirculation) can be derived with the same method. Then it is necessary to differentiate between the air ratio (n) and the oxygen ratio (n<sub>s</sub>). The latter is described as the ratio between the amount of oxygen input and the stoichiometric oxygen requirement of the furnace.

All derived equations are valid for the full oxidation of the component C, H and S. In reality, fuels may contain other components which perform chemical reactions (e.g. Cl and F). Actually, this need to be considered in the elementary combustion calculation and the equation need to be adapted. However, since the Cl- and F- content of practical fuels are generally low, this small error may be accepted.

## A2) Process simulation of the 20 kW lab-scale BFBC with Aspen Plus®

Aspen Plus is a process simulator that predicts the behavior of chemical reactions and steps using standard engineering relationships, such as mass and energy balances, rate correlations, as well as phase and chemical equilibrium data [2]. By choosing the appropriate unit operations and thermodynamic models, reliable thermodynamic data and realistic operating conditions, Aspen Plus uses mathematical models to predict the performance of the cycle and actual plant behavior.

In the current study, a simplified process model of the 20 kW BFBC has been constructed and subsequently validated. A schematic of the model used for the investigation of SRF combustion under air-firing conditions is introduced in Figure 16. Schematic of the simplified 20 kW BFBC simulation model and a description of the operation units in Table 8. Description of the process units included in the 20 kW BFBC simulation model.

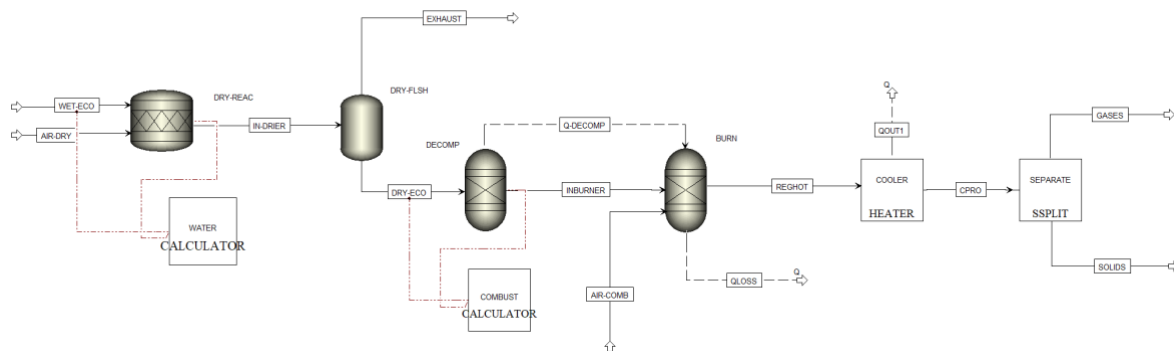


**Figure 16.** Schematic of the simplified 20 kW BFBC simulation model

**Table 8.** Description of the process units included in the 20 kW BFBC simulation model [3]

Op. Unit	Type	Description
DRY-REAC	Reactor	It models the drying of the fuel according to a drying calculator.

DRY-FLSH	Separator	Isobaric and adiabatic humidity separator.
DECOMP	Reactor	Required for decomposing a non-conventional fuel (e.g. waste) into its constituent elements. The heat of reaction associated with the decomposition of the fuel is considered in the combustion process (BURN). The yield needs to be specified (by a calculator block), but it does not require reaction stoichiometry and kinetics.
BURN	Reactor	It is used to model reactions that come to chemical equilibrium (e.g. combustion). It calculates the chemical and phase equilibrium by minimising the Gibbs free energy of the system. The reaction stoichiometry does not need to be specified.
COOLER	Exchanger	It cools the gas after combustion. It requires two thermodynamic specifications (i.e. temperature and pressure).
SEPARATE	Splitter	It allows the separation of the cooled flue gas from the solid ash. It only requires the separation efficiency of the desired fraction (i.e. solid or gas).
HUMIDITY	Calculator	It specifies the moisture content of the dried fuel and calculates the corresponding conversion of fuel to water. The material balance equations for this process define relations between the following quantities: i) water content of the feed fuel; ii) fractional conversion of fuel to water; iii) water content of the dried fuel.
COMBUST	Calculator	It calculates the actual yield distribution from the component attributes for fuel in the feed stream to DECOMP.

For the oxy-fuel combustion model a similar schematic is used. Since flue gas recirculation is not available at the 20 kW BFB facility, the oxy-fuel oxidising gas is simulated with O<sub>2</sub> and CO<sub>2</sub> (mainly), together with a small amount of N<sub>2</sub> required for flushing purposes in the facility. This is reflected in the model, where the “AIR-COMB” stream in this case is replaced by a gas mixture containing the three above mentioned species. As for the rest of the model (i.e. operation units) no further changes are required, apart from the adjustment of common process streams (i.e. WET-ECO and AIR-DRY).